Review paper

Spectroscopic imaging at compact inverse Compton X-ray sources

Stephanie Kulpe [a,*], Martin Dierolf [a], Benedikt Günther [a], Johannes Brantl [a], Madleen Busse [a], Klaus Achterhold [a], Franz Pfeiffer [a,b], Daniela Pfeiffer [b]

[a] *Chair of Biomedical Physics, Department of Physics and Munich School of BioEngineering, Technical University of Munich, James-Franck-Str. 1, 85748 Garching, Germany*
[b] *Department of Diagnostic and Interventional Radiology, Munich School of Medicine and Klinikum rechts der Isar, Ismaniger Str. 22, 81675 Munich, Germany*

ABSTRACT

While K-edge subtraction (KES) imaging is a commonly applied technique at synchrotron sources, the application of this imaging method in clinical imaging is limited although results have shown its superiority to conventional clinical subtraction imaging. Over the past decades, compact synchrotron X-ray sources, based on inverse Compton scattering, have been developed to fill the gap between conventional X-ray tubes and synchrotron facilities. These so called inverse Compton sources (ICSs) provide a tunable, quasi-monochromatic X-ray beam in a laboratory setting with reduced spatial and financial requirements. This allows for the transfer of imaging techniques that have been limited to synchrotrons until now, like KES imaging, into a laboratory environment. This review article presents the first studies that have successfully performed KES at ICSs. These have shown that KES provides improved image quality in comparison to conventional X-ray imaging. The results indicate that medical imaging could benefit from monochromatic imaging and KES techniques. Currently, the clinical application of KES is limited by the low K-edge energy of available iodine contrast agents. However, several ICSs are under development or already in commissioning which will provide monochromatic X-ray beams with higher X-ray energies and will enable KES using high-Z elements as contrast media. With these developments, KES at an ICS has the ability to become an important tool in pre-clinical research and potentially advancing existing clinical imaging techniques.

1. Introduction

In conventional X-ray imaging, the image contrast arises from variations in absorption of different materials or tissues. Thereby, the X-ray absorption is dependent on the elemental composition and density of the material. However, the elemental composition of soft tissues is rather similar, leading to a weak attenuation contrast. In subtraction X-ray imaging, tissue structures or organs are visualized using a contrast agent that changes the attenuation between the contrasted structure and the surrounding tissue [1]. Digital subtraction angiography (DSA) is a clinically well-established fluoroscopy technique in interventional angiography, which allows for improved visualization of the blood vessels by using a temporal subtraction technique [2]. In this procedure, a reference image without contrast agent is subtracted from all subsequent contrast enhanced images in order to remove background structures and therefore improve the visibility of contrast enhanced vessels. However, artifacts from patient movement, breathing and cardiac motion may have a negative impact on image quality [3,4].

K-edge subtraction (KES) imaging exploits the sharp increase of the absorption coefficient of a contrast agent to acquire images at energies just below and above the K-edge energy. In contrast to DSA, where X-ray images are taken before and after the injection of the iodine contrast agent, images in KES imaging are both taken after the injection, but at different X-ray energies. Elleaume et al. [5] showed that this makes the method more suitable for imaging moving organs. KES imaging was performed at conventional polychromatic laboratory sources using a Ross filter arrangement [6] or a multi-bin photon counting detector [7,8]. However, when using filters, a large amount of the X-ray beam is absorbed, which leads to long acquisition times and limits the acquisition speed. For multi-bin photon counting detectors the energy threshold resolutions is usually 1–2 keV, which limits the ability to acquire images closely around the K-edge. Due to these disadvantages, KES has mainly been applied at synchrotron facilities in the past. While spectral filtering of synchrotron radiation provides highly brilliant, monochromatic X-rays, synchrotrons rely on electron storage rings

* Corresponding author.
  E-mail address: stephanie.kulpe@tum.de (S. Kulpe).

of several hundred meters in circumference and are expensive in terms of installation as well as operation and maintenance. In contrast, the use of conventional X-ray tubes in laboratories and hospitals is comparably cheap, but they have low brilliance and polychromatic X-ray spectra. A conventional X-ray spectrum will be modified as it traverses the patient, since lower energies are attenuated more strongly than higher ones. This beam hardening impairs the measurement accuracy and can interfere with the goal to optimize both dose level and image quality [9,10]. As K-edge subtraction imaging works best using a monochromatic X-ray beam, its feasibility in clinical routine has been limited. Over the past decades, compact X-ray sources, based on the principle of inverse Compton scattering, have been emerging to fill the gap between laboratory sources and synchrotron facilities and provide a tunable, monochromatic X-ray beam in a laboratory frame [11–14]. These inverse Compton sources (ICSs) provide X-ray beams with a brilliance in between those of a large-scale synchrotron and a conventional X-ray source. For example, the ICS installed at the Munich Compact Light Source (MuCLS) provides high-intensity X-rays that are quasi-monochromatic and are emitted into a much smaller opening angle than at an X-ray tube, thereby providing a brilliance of ~1.2×10^{10} photons s^{-1} mm^{-2} mrad^{-2} $(0.1\%\,\mathrm{BW})^{-1}$ [15] in comparison to a standard rotating anode with ~0.6×10^{9} photons s^{-1} mm^{-2} mrad^{-2} [16] and a third generation synchrotron ~10^{21} photons s^{-1} mm^{-2} mrad^{-2} $(0.1\%\,\mathrm{BW})^{-1}$ [17]. Other ICSs provide, or are expected to provide, similar brilliances in the order of 10^{10} photons s^{-1} mm^{-2} mrad^{-2} $(0.1\%\,\mathrm{BW})^{-1}$ such as TTX [18] or ThomX [19,12]. Compared to the synchrotron facilities, a main advantage of ICSs are the reduced spatial and financial requirements [11,12,14] for acquisition, operation and maintenance. These lower costs enable the transfer of certain techniques that have been limited to synchrotrons so far, like KES-imaging, into a laboratory or pre-clinical setting.

This review article gives an overview over the working principles of inverse Compton X-ray sources and work on K-edge subtraction imaging for medical applications. While many ICSs are under development, only few are operational and producing results. Therefore, most of the biomedical KES results discussed here were produced at the Munich Compact Light Source (MuCLS).

2. Inverse Compton sources

There are several ongoing projects developing, constructing or running a compact X-ray source based on the principle of inverse Compton scattering, where high energy electrons interact with laser photons to produce X-rays. Basically, there are two different setups (cf. Fig. 1): on the one hand, a linac-based design (e.g., STAR [13,20], LCS at AIST [21], the Compton source at BNL ATF [22], TTX [23,24], Smart*Light [25], the ASU-ICS-project [26] as well as the proposed

inverse Compton sources at MIT [27] and BriXS [28]). On the other hand, a storage ring-based design (e.g. at MuCLS [14], ThomX [19,12] and NESTOR [29,30]). In a linac-based setup, the electrons are produced by a photo-cathode radio-frequency (RF) gun and are subsequently accelerated in a linear accelerator (linac) to relativistic energies and collide with laser photons. In a storage ring-based setup, the accelerated electrons are injected into an electron storage ring. In the storage ring, the electron bunch circulates with a high revolution frequency and is replaced from time to time to ensure high beam quality. To generate high-power laser pulses at a equally high repetition rate, usually a passive laser enhancement cavity is used. In one point in the electron storage ring (or in the linac-based design: in one point of the linear beam path), the counter-propagating electron bunches interact with the laser pulses in the process described below. Their repetition rates are matched so that electrons and laser photons collide upon each revolution at the interaction point producing a narrow cone beam of X-rays.

There are two different, but fully equivalent, descriptions of the X-ray production at a compact synchrotron X-ray source. In the particle view, the X-ray production at a compact synchrotron source can be explained with the process of inverse Compton scattering. A relativistic electron collides with a photon of a high intensity laser pulse, changing the momenta of both electron and laser photon. The photon is back-scattered and emerges with a much shorter wavelength (see Fig. 2). The relation between the scattered photon energy E to the incident laser photon energy E_L and electron energy $\mathscr{E}$ can be written as, assuming $E_L \ll m_0 c^2$ and a Lorentz factor $\gamma \gg 1$ [12],

$$E = \frac{2\gamma^2 E_L (1 - \cos(\theta_1))}{1 + \gamma^2 \theta_2^2}, \tag{1}$$

with θ_1 the angle between relativistic electron and laser photon and θ_2
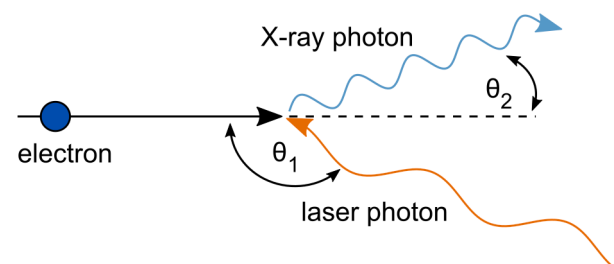
Fig. 2. Principle of inverse Compton scattering: A laser photon is scattered at a relativistic electron at an angle of θ_1. The scattered photon has a higher energy and propagates under the angle θ_2. For better understanding, the angles are exaggerated.
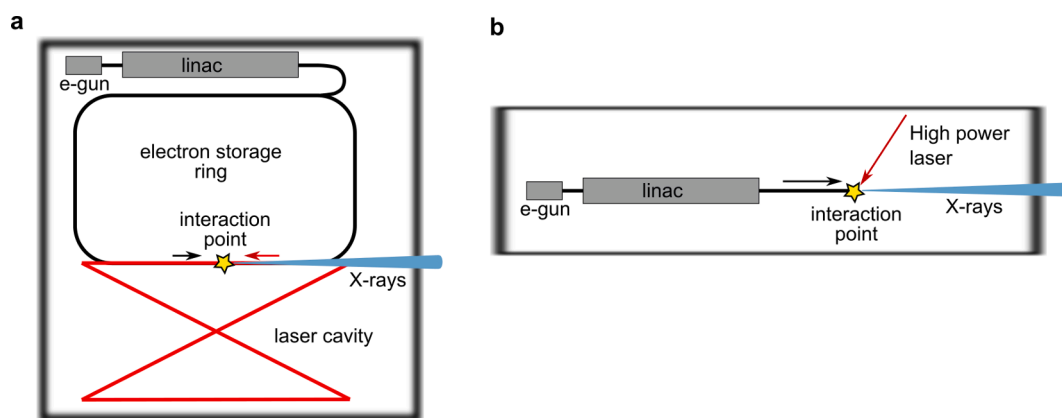
Fig. 1. Schematics of inverse Compton sources with (**a**) and without (**b**) electron storage ring. The electrons are emitted by the electron gun and accelerated to relativistic energies in the linear accelerator (linac). The electrons interact with the laser photons in the interaction point and generate X-rays in the process of inverse Compton scattering. The setup in **a** shows the ICS at the MuCLS where the laser is enhanced in a bow-tie shaped, high-finesse cavity [14].

the angle of the scattered photon.

In the wave picture, the counter-propagating laser photons act as a localized electromagnetic field on the electrons, analog to a permanent magnetic undulator [31]. For undulator radiation, the basic parameters are the undulator period λ_u and the Lorentz factor γ which relates to the electron energy. The undulator period λ_u corresponds to half of the laser wavelength, i.e., about 0.5 µm for typical infrared lasers based on Neodymium or Ytterbium. This period is about 10^4 times smaller than at a synchrotron facility (λ_u~ cm), which allows to reduce the electron energy by a factor of 100 and thus also to scale down the electron storage ring to a few meters in circumference. This enables the inverse Compton source to fit into a standard laboratory [14].

The X-ray flux, thus the number of emitted X-rays per second, for a head-on inverse Compton scattering of electron bunches and laser pulses can be calculated as [12,32]

$$F_{tot} = \frac{\sigma_T N_L N_e f_{rep}}{2\pi(\sigma_e^2 + \sigma_l^2)},$$
(2)

where σ_T is the Thomson cross-section, N_e is the number of electrons per bunch, N_L the number of photons per laser pulse, f_{rep} the repetition frequency of electron-laser interactions, σ_e the transverse size of the electron bunch and σ_L the transverse size of the laser pulse at the interaction point. The X-ray flux can be increased by decreasing the source size, increasing the number of photons and electrons or by using a higher repetition frequency. While a storage ring design results in a f_{rep} in the MHz range, it is usually much lower for linac-based ICSs, which in turn have a higher X-ray flux per individual collision.

3. K-edge subtraction imaging (KES)

3.1. History of K-edge subtraction imaging at synchrotron sources

The principle of KES was first suggested by B. Jacobson [33] in 1953, who proposed the use of monochromatic X-rays to increase contrast in absorption imaging. His idea was to take advantage of the differences in absorption of two or more monochromatic X-ray beams to produce an image only showing these differences and/or the concentration of an element in an object. The first studies of KES were performed by Rubenstein et al. [34,35] at the Stanford Synchrotron Radiation Laboratory demonstrating the feasibility of coronary angiography. The first *in vivo* KES images were made of the coronary arteries of an anesthetized dog [36]. In the early days of KES, its main application was coronary angiography, since there were great struggles in DSA to get artifact free images [3] and to safely perform the invasive procedures also concerning the use of high doses of contrast agent [37,38]. The developments in KES led to first results of human patients [38,39]. Elleaume et al. thereby showed that KES coronary angiography at synchrotrons provides improved image quality in comparison to DSA at a conventional X-ray source while reducing the risk for the patient using transvenous injection of contrast agent instead of an interventional procedure [40]. Afterwards, several other studies were performed demonstrating the benefits of KES for coronary [41,42] and neurovascular angiography [43]. At the same time, KES was also applied in computed tomography [44,45]. However, the application of KES at synchrotrons has not been limited to angiography. Also, studies on functional lung imaging [46,47] and bone growth and disease have been conducted [48,49]. An extensive review of KES at synchrotrons was written by Thomlinson et al. [1].

While the studies performed at synchrotron sources have shown very promising results, the application of KES in clinical routine is restricted due to the limited accessibility of synchrotron facilities. Therefore, compact synchrotron sources could enable KES imaging in a pre-clinical setting.

3.2. KES formalism with two energies

This formalism assumes two monochromatic X-ray beams with energies bracketing the K-edge of the used contrast agent that penetrate the sample volume completely and are detected separately and simultaneously. A discussion for a setup using an X-ray filter to manipulate the energy of a quasi-monochromatic X-ray beam can be found in [50].

The number of photons $N(E_\pm)$ detected by the detector is [51]

$$N(E_\pm) = N_0(E_\pm)\exp\left[-\sum_j \left(\frac{\mu}{\rho}(E_\pm)(\rho t)\right)_j\right] + D$$
(3)

where $N_0(E_\pm)$ is the number of incident photons per pixel with energies E_- below and E_+ above the K-edge of the contrast agent, μ/ρ the mass attenuation coefficient, ρ the density of the material, t the path length and D the dark current of the detector. The index j denotes the different materials and tissues (i.e., contrast agent, bone and soft tissue). The sample can be decomposed into two basis materials, usually "contrast agent/iodine" and "tissue", using the dual-energy method by Lehmann et al. [52]

$$\ln\frac{N_0}{N}(E_\pm) = \left[\frac{\mu}{\rho}(E_\pm)(\rho t)\right]_{iodine} + \left[\frac{\mu}{\rho}(E_\pm)(\rho t)\right]_{tissue}$$
(4)

where μ/ρ_{iodine} is the mass attenuation coefficient of the iodine contrast agent and μ/ρ_{tissue} is the mass attenuation coefficient of all other materials excluding the contrast agent. $N_0(E_\pm)$ are calculated by using the flat fields, i.e., the images at two different energies acquired without sample. The dark current D is subtracted from the flat field images before applying the dual-energy method. Tabulated values are used for the mass attenuation coefficients μ/ρ of contrast agent and tissue. The mass densities of contrast agent $(\rho t)_{iodine}$ and of tissue $(\rho t)_{tissue}$ are calculated by solving the two logarithmic expressions of Eq. (4)

$$(\rho t)_{iodine} = \frac{\left[\frac{\mu}{\rho}(E_-)\right]_{tissue}\ln\frac{N_0}{N}(E_+) - \left[\frac{\mu}{\rho}(E_+)\right]_{tissue}\ln\frac{N_0}{N}(E_-)}{\left[\frac{\mu}{\rho}(E_-)\right]_{tissue}\left[\frac{\mu}{\rho}(E_+)\right]_{iodine} - \left[\frac{\mu}{\rho}(E_+)\right]_{tissue}\left[\frac{\mu}{\rho}(E_-)\right]_{iodine}}$$
(5)

$$(\rho t)_{tissue} = \frac{\left[\frac{\mu}{\rho}(E_+)\right]_{iodine}\ln\frac{N_0}{N}(E_-) - \left[\frac{\mu}{\rho}(E_-)\right]_{iodine}\ln\frac{N_0}{N}(E_+)}{\left[\frac{\mu}{\rho}(E_-)\right]_{tissue}\left[\frac{\mu}{\rho}(E_+)\right]_{iodine} - \left[\frac{\mu}{\rho}(E_+)\right]_{tissue}\left[\frac{\mu}{\rho}(E_-)\right]_{iodine}}.$$
(6)

3.3. Change in CNR due to energy spread in ICS spectrum

The CNR in the KES image is dependent on the difference of the mean absorption and thus the difference of the mean absorption coefficients $\Delta\mu$ of the sample at the two energies above and below the K-edge,

$$\text{CNR} = \frac{\Delta\mu}{\sigma},$$
(7)

where σ is the standard deviation in a background region. In general, the energy spread of ICS sources will lead to a lower mean energy of the spectrum compared to its peak energy due to its broad low energy tail. While this increases the mean absorption coefficient of the low energy image, it decreases the one of the high energy image for peak energies of the spectra tuned below and above the material's K-edge. Therefore, their difference will be reduced, which results in a reduction of the contrast in the K-edge subtraction image. In other words, the CNR for KES-images obtained from quasi-monochromatic ICS spectra is decreased compared to the monochromatic case. The exact difference depends on the used X-ray spectra. The intensity I of the spectrum which is transmitted through the sample can be described by

$$I = \int f(E)\cdot I_0\cdot\exp^{-\mu(E)d}\,dE, \text{ with } \int f(E) = 1,$$
(8)

where I_0 is the incident intensity of the X-ray beam, $\mu(E)$ is the attenu-

ation coefficient dependent on the energy E, d is the thickness of the sample and $f(E)$ give the proportional contribution of each energy to the intensity of the spectrum. This formula yields the aforementioned effective mean absorption coefficient for the high or low energy image, respectively.

A study by Sarnelli et al. [53] compared the signal-to-noise ratio (SNR) in images obtained at a synchrotron to the SNR of images obtained at a monochromatized conventional X-ray source. A positive impact on the image SNR was found for a smaller energy difference, which is achievable with a more narrow monochromatic beam. However, even with large energy differences between the images, good material separation was obtained.

4. KES applications in biomedical research at inverse Compton X-ray sources

While K-edge filtering at ICSs has been used for characterization of the X-ray source and the measurement of the local X-ray spectrum [54,55], the properties of ICSs' monochromatic X-ray spectra have been shown to be beneficial for biomedical imaging. The first experiments showing the benefit of monochromatic X-rays produced at a compact X-ray source were performed by Carroll et al. in 2003 [56]. In their study, they compared images from breast and finger phantoms and a mouse pelvis which were taken with conventional polychromatic spectra and with the monochromatic X-ray beam produced at an ICS at Vanderbilt University. The monochromatic images of the breast phantom thereby provided better image quality than the conventional images and allowed for the identification of more lesions in the tissue. The benefits of monochromatic X-rays produced by ICSs were affirmed in further studies by Yamada et al. [57] and Kuroda et al. [21] at the LCS, focusing on refraction and phase-contrast imaging of bones. A major advantage of ICSs in comparison to conventional sources is that the spectrum can be tuned to the K-edge of the applied contrast agent. This provides a higher contrast in the acquired images [57,58]. Carroll showed the improvement in signal due to the higher X-ray absorption by the iodine contrast agent when tuning the X-ray beam directly to the K-edge and discussed its application for molecular and cellular imaging and therapy [59]. A study of KES using barium sulfate as a contrast agent was conducted by Kuroda et al. [60]. They demonstrated the feasibility of the imaging technique using a human head phantom at the LCS at AIST. Although the volume concentration ratio of the contrast agent was only 3%, the contrast enhancement was seen to be 5%. Another comparison of imaging with poly- and monochromatic spectra was performed by Eggl et al. [58]. They analyzed the quantitative effect of quasi monoenergetic X-ray spectra on the CNR of coronary angiography. For this, they used virtual projection images calculated from segmented real patient data of a human coronary artery and compared a typical clinical X-ray spectrum with a compact synchrotron spectrum. For an iodine-based contrast agent, a conventional X-ray tube spectrum at 60 kVp was compared to a quasi monoenergetic spectrum at 35 keV. Additionally, a 90 kVp conventional X-ray tube spectrum and a 55 keV quasi monoenergetic spectrum were examined for the application of gadolinium-based contrast media. The CNR analysis showed that the CNR values were 17–22% higher in the monoenergetic images than the values for the conventional spectra. For lower concentrations of contrast agent, the advantage of monoenergetic imaging increases further, suggesting that a monoenergetic spectrum would allow for a reduction of the iodine concentration by approximately 20–30% at equal CNR, which can facilitate the administration of the contrast agent for the patients. For the simulations with gadolinium, similar results were obtained, with an even larger improvement in CNR.

However, the advantages of monoenergetic imaging are not limited to projection imaging. Also for three dimensional imaging, monoenergetic imaging provides benefits. In a study, Achterhold et al. compared computed tomographies (CTs) obtained with an ICS and a conventional X-ray tube [75]. The experimental results obtained for

quantitative CT measurements of mass absorption coefficients in a water phantom sample confirmed that images from an ICS can yield much higher CT image quality, particularly concerning quantitative aspects of CT imaging. Several other studies also confirmed that the application of monochromatic CT yields more precise determination of density values in the sample [61,62].

Already in 2002, the application of KES imaging at an ICS was discussed as a possibility to bring monochromatic imaging into a clinical context, improve diagnostic techniques and develop new types of therapy [63]. However, only in 2018, the first biomedical KES experiments were performed at the Munich Compact Light Source (MuCLS). Here, a filter-based KES approach was implemented and its feasibility proven both in a phantom study and on an excised porcine heart. The proof-of-principle study showed that KES imaging is in principle possible at an ICS, levels out differences in absorption and separates the contrast agent from the background structures (cf. Fig. 3). Additionally, the results confirmed the findings from synchrotron sources that KES imaging can improve the visibility of blood vessels overlaid by bone structures. A CNR study confirmed the visual impression of improved visibility. The CNR between the blood vessel behind the rib and the rib bone was calculated to 0.44 ± 0.52 in the non-subtraction image (cf. Fig. 3a), and therefore the signal lies below the noise level, whereas the corresponding CNR is 5.16 ± 0.53 in the KES image (cf. Fig. 3b) [50].

Another study [64] concentrated on the issue in clinical radiography that iodine contrast agent cannot be distinguished from calcification since the attenuation values of iodine and calcium are usually very similar or even identical. To demonstrate the ability of KES to separate iodine and calcium in projection imaging, both a study with a phantom containing the two materials and a study of a human carotid artery with calcification and a sodium iodide solution were carried out. In both studies, the separation of the two materials was successfully performed, thereby calculating images only showing one of the two materials. These experiments showed that KES imaging at a compact synchrotron source enables the differentiation of iodine contrast agent from calcium.

To evaluate if the advantages of KES also apply in 3D imaging, a CT study was conducted [65]. In this study, two CT scans were performed of an excised porcine kidney containing a calcified kidney stone at different mean energies. Due to the change in the attenuation coefficient of the iodine contrast agent between the two scans, it was possible to completely separate calcium and iodine and calculate CT volumes only containing one of the two materials (cf. Fig. 4). KES CT can therefore provide additional diagnostic information which could be of special interest in various clinical use cases like kidney stones, atherosclerosis and bone imaging.

The most recent study addressed the advantage of KES in imaging moving organs in comparison to the clinically used digital subtraction angiography. The authors evaluated a filter-based KES fluoroscopy application and compared its performance to conventional temporal subtraction at the MuCLS. For this, iodine contrast agent was injected into an *ex vivo* mouse while acquiring X-ray projection images. From the acquired images, KES and conventional temporal subtraction images were calculated. At the same time, movement of the sample was simulated to demonstrate the appearance of motion artifacts commonly observed in *in vivo* conventional temporal subtraction imaging. The results suggest that K-edge subtraction imaging at a compact synchrotron source can provide images with improved visibility of contrasted structures in comparison to conventional non-subtraction X-ray images and with reduced artifacts compared to conventional temporal subtraction (cf. Fig. 5). The CNR was significantly higher in the KES images compared to the unfiltered non-subtraction images (300–770%) and between 14.9% (between backbone and contrast agent) and 21.5% (between ribs and contrast agent) higher than in the conventional temporal subtraction images. The observed benefits of KES could enable subtraction imaging in future medical applications, e.g. of the gastrointestinal tract [66].
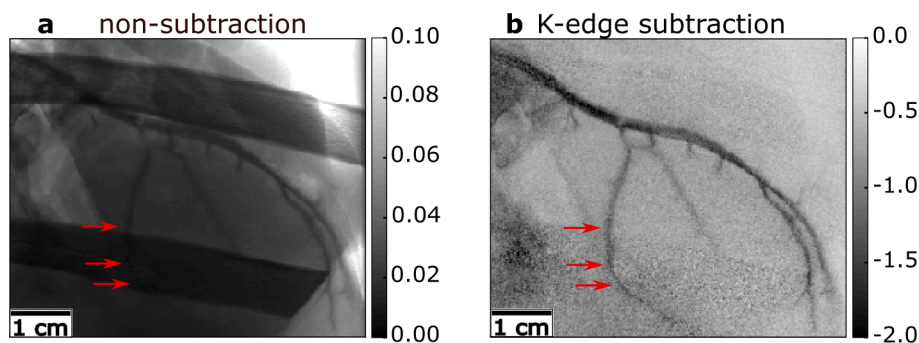
Fig. 3. Projection images of an excised porcine heart embedded in a rib cage. **a** Monochromatic X-ray image of coronary arteries overlaid by bones of rib cage. Especially the visibility of smaller vessels is compromised; **b** KES image of the same sample. KES levels out differences in absorption and separates the contrast agent from the background structures. The visibility of the blood vessels is increased, especially for those previously overlaid by bone structures. The gray scale for the non-subtraction image shows the relative intensity/transmission of the X-ray beam, while the gray values in the KES image show the negative logarithmic differences in the absorption. Figure adapted from [50].
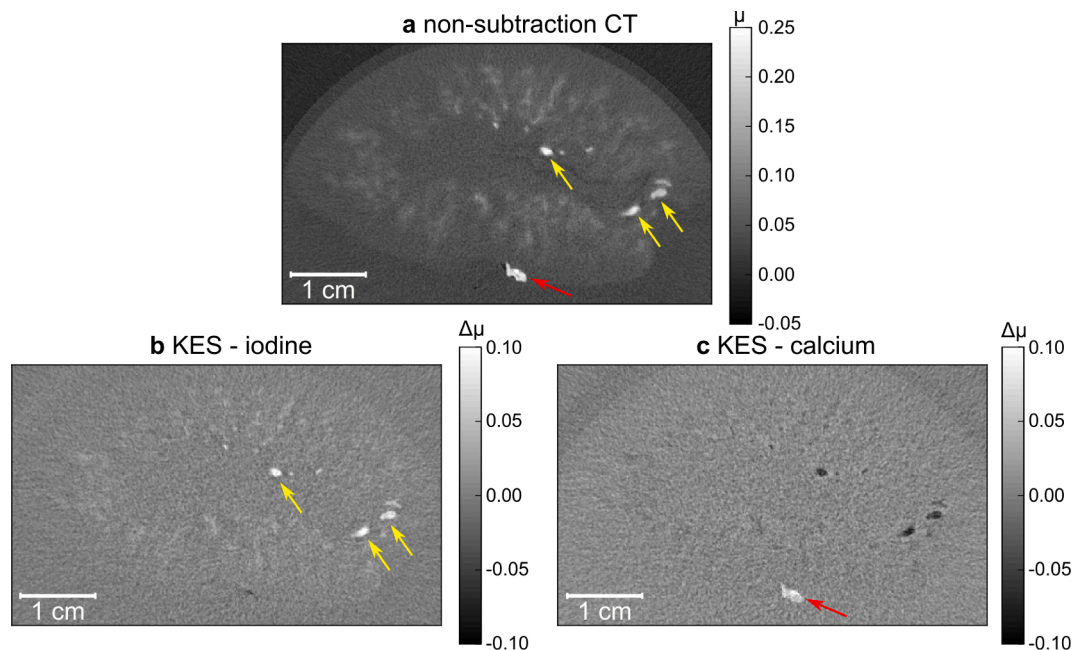
Fig. 4. Reconstructed CT slices of porcine kidney with kidney stone (indicated by the red arrow) in transverse slice orientation. **a** Non-subtraction CT slice, where both the blood vessels (indicated by the yellow arrows) and the kidney stone are visible; **b** In the KES image only structures containing iodine contrast agent stay visible, the kidney stone is eliminated from the image; **c** When performing inverse KES, the iodine is inverted so that the kidney stone can be clearly identified. The gray scales of the conventional CT slice show the absorption values in 1/mm whilst the KES slices show the differences in absorption. This figure is part of a figure previously published in [65] under a CC-BY license (http://creativecommons.org/licenses/by/4.0/). (For interpretation of the references to color in this figure legend, the reader is referred to the web version of this article.)

5. Future developments

In a simulation study, Paterno et al. [67] evaluated the applicability of KES at ICSs for a realistic dilution of the iodine contrast agent in arteries and the projected beam parameters of the proposed BriXS project [28]. They found that ICSs have to deliver a fluence of 10^8 ph/mm^2 at the sample plane to image most arteries with sufficient contrast and acquisition times of a few hundred milliseconds, which is significantly higher than demonstrated up to now. Moreover, experimental KES studies at ICSs had been limited to iodine or barium, i.e., an X-ray range well below 40 keV due to the ICSs' energy range. At this energy, the absorption of the X-rays in the human body is very high. This leads to a high absorbed dose and limits the penetrable tissue thickness.

Consequently, the X-ray flux as well as maximum energy of the compact synchrotron X-ray sources have to increase to enable KES imaging in a clinical setting. At the MuCLS, the former could be addressed with improvements of the laser enhancement cavity, while the latter could be achieved by replacing the infrared laser with a visible light one. Alternatively, the electron acceleration system could be designed for higher energy electrons. This route was chosen for several inverse

Compton sources currently under development or construction that aim at higher X-ray energies as well as X-ray fluence to enable KES imaging at clinically relevant energies in the future. One of these sources is ThomX which is under construction in Orsay, France and is expected to start operation in 2020. There, KES experiments for the determination of contrast agent concentrations are planned [19]. Additionally, ThomX could be used to investigate high-Z element drugs since the source provides an X-ray beam with X-ray energies of up to 90 keV [12,68]. In order to allow fast energy switching for KES without the need of absorption filters, two approaches are suggested in the proposal for BriXS [28]: Either the use of two laser systems or rapid adjustment of the laser-electron collision angle [69].

As iodine is not an efficient contrast agent at these X-ray energies, different ones have to be used or developed for optimal performance of KES. In the past, studies have shown that gadolinium contrast agent, which is commonly used in MRI imaging today, could also be used in X-ray imaging [70,71], especially for patients with renal insufficiency [72,73]. The gadolinium K-edge is at 50.2 keV, which would allow for dose compatible KES imaging on the human body. However, recent studies have questioned the safety of gadolinium as a contrast agent
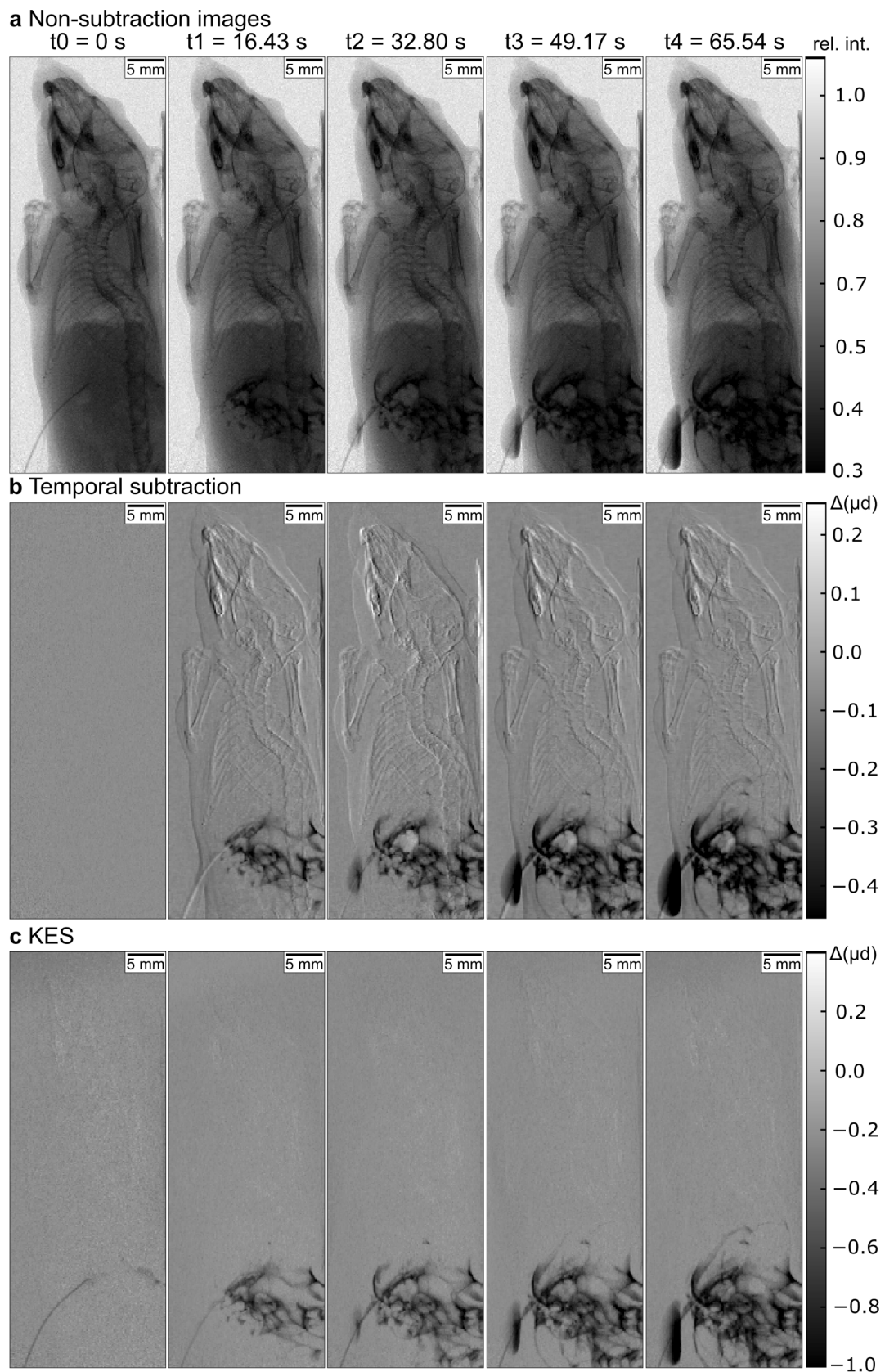
Fig. 5. a Conventional non-subtraction image; **b** temporal subtraction image, due to the temporal delay between the images, artifacts occur in the subtraction process; **c** KES image, here there are no artifacts since two subsequently acquired images are subtracted. The gray scales for the unfiltered images display the relative intensity/ transmission of the X-ray beam, while the gray values in the KES and conventional temporal subtraction images show the negative differences in the absorption. This figure was previously published in [66] under a CC-BY license (http://creativecommons.org/licenses/by/4.0/).

[74]. With high X-ray energy ICSs becoming operational in the near future, the application of KES based on alternative high-Z contrast agents could become possible, which would pave the way for KES in a clinical environment.

6. Conclusion

Studies at different ICSs have shown that KES imaging is not limited to synchrotron sources, but can be made available in a laboratory frame. The results indicate that medical imaging could benefit from monochromatic imaging and that K-edge subtraction techniques can improve image quality which could facilitate diagnosis. Presently, the application in medical imaging is limited by the low K-edge of the available contrast agents and the strong X-ray absorption in the human body at this energy. In the future, this issue can be overcome by the development of new contrast agents with higher K-edge energies, such as gadolinium. Currently, several ICSs are under development or already in commissioning which will provide monochromatic X-ray beams with higher X-ray energies, which will enable KES using high-Z elements as contrast media. With these developments, KES at an ICS has the ability to become an important tool in pre-clinical research and potentially advancing existing clinical imaging techniques.

References

[1] Thomlinson W, Elleaume H, Porra L, Suortti P. K-edge subtraction synchrotron X-ray imaging in bio-medical research. Physica Med 2018;49:58–76. https://doi.org/10.1016/j.ejmp.2018.04.389.

[2] Meijering EHW, Zuiderveld KJ, Viergever MA. Image registration for digital subtraction angiography. Int J Comput Vision 1999;31:227–46. https://doi.org/10.1023/A:1008074100927.

[3] Tobis JM, Nalcioglu O, Henry WL. Digital subtraction angiography. Chest 1983;84 (1):63–86. https://doi.org/10.1016/j.cognition.2008.05.007.

[4] Yamamoto M, Okura Y, Ishihara M, Kagemoto M, Harada K, Ishida T. Development of digital subtraction angiography for coronary artery. J Digit Imaging 2009;22(3):319–25. https://doi.org/10.1007/s10278-008-9108-1.

[5] Elleaume H, Charvet AM, Corde S, Estève F, Le Bas JF. Performance of computed tomography for contrast agent concentration measurements with monochromatic x-ray beams: comparison of K-edge versus temporal subtraction. Phys Med Biol 2002;47:3369–85. https://doi.org/10.1088/0031-9155/47/18/307.

[6] Arhatari BD, Gureyev TE, Abbey B. Elemental contrast X-ray tomography using Ross filter pairs with a polychromatic laboratory source. Sci Rep 2017;7:218. https://doi.org/10.1038/s41598-017-00304-7.

[7] Roessl E, Proksa R. K-edge imaging in x-ray computed tomography using multi-bin photon counting detectors. Phys Med Biol 2007;52:4679–96. https://doi.org/10.1088/0031-9155/52/15/020.

[8] Schlomka JP, Roessl E, Dorscheid R, Dill S, Martens G, Istel T, Bäumer C, Herrmann C, Steadman R, Zeitler G, Livne A, Proksa R. Experimental feasibility of multi-energy photon-counting K-edge imaging in pre-clinical computed tomography. Phys Med Biol 2008;53:4031–47. https://doi.org/10.1088/0031-9155/53/15/002.

[9] Brooks RA, Di Chiro G. Beam hardening in X-ray reconstructive tomography. Phys Med Biol 1976;21(3):390–8. https://doi.org/10.1088/0031-9155/21/3/004.

[10] Boas FE, Fleischmann D. CT artifacts: Causes and reduction techniques. Imag Med 2012;4(2):229–40. https://doi.org/10.2217/iim.12.13.

[11] Huang Z, Ruth RD. Laser-electron storage ring. Phys Rev Lett 1998;80(5):976–9. https://doi.org/10.1103/physrevlett.80.976.

[12] Jacquet M. High intensity compact Compton X-ray sources: Challenges and potential of applications. Nucl Instrum Meth Phys Res B 2014;331:1–5. https://doi.org/10.1016/j.nimb.2013.10.078.

[13] Bacci A, Agostino R, Alesini D, Barberis R, Bellaveglia M, Beltrano J. Status of the STAR Project. In Proceedings of IPAC2016, Busan, Korea, Vol. TUPOW004; 2016. p. 1747–50. doi:10.18429/JACoW-IPAC2016-TUPOW004.

[14] Eggl E, Dierolf M, Achterhold K, Jud C, Günther B, Braig E, Gleich B, Pfeiffer F. The munich compact light source: initial performance measures. J Synch Radiat 2016;23(5):91–100. https://doi.org/10.1107/S160057751600967X.

[15] Günther B, Gradl R, Jud C, Eggl E, Huang J, Kulpe S, Achterhold K, Gleich B, Dierolf M, Pfeiffer F. The versatile X-ray beamline of the munich compact light source: design, instrumentation and applications. J Synch Radiat 2020;27. https://doi.org/10.1107/S1600577520008309.

[16] Skarzynski T. Collecting data in the home laboratory: Evolution of X-ray sources, detectors and working practices. Acta Crystallogr Sect D 2013;69(7):1283–8. https://doi.org/10.1107/S0907444913013619.

[17] Balewski K, Brefeld W, Decking W, Franz H, Weckert E. PETRA III: a low emittance synchrotron radiation source technical design report, Tech. rep., DESY, Hamburg, Germany (2004). URL https://bib-pubdb1.desy.de/record/369752.

[18] Yu P, Huang W. Lattice design and beam dynamics in a compact X-ray source based on Compton scattering. Nucl Instrum Meth Phys Res Sec A 2008;592(1–2):1–8. https://doi.org/10.1016/j.nima.2008.03.114.

[19] Variola A, The ThomX Project. In 2nd international particle accelerator conference (IPAC'11), Sep 2011, San Sebastian, Spain, vol. in2p3-0063; 2011. p. 1903–5. http://hal.in2p3.fr/in2p3-00635646.

[20] Faillace L, Agostino RG, Bacci A, Barberi R, Bosotti A, Broggi F, et al. Status of compact inverse Compton sources in Italy: BriXS and STAR. In Proc. SPIE 11110, advances in laboratory-based x-ray sources, optics, and applications vii, spie optical engineering + applications, 2019, San Diego, California, United States, vol. 1111005; 2019. p. 4. doi:10.1117/12.2531168.

[21] Kuroda R, Toyokawa H, Yasumoto M, Ikeura-Sekiguchi H, Koike M, Yamada K, Yanagida T, Nakajyo T, Sakai F, Mori K. Quasi-monochromatic hard X-ray source via laser Compton scattering and its application. Nucl Instrum Meth Phys Res Sec A 2011;637(1 SUPPL.):S183–6. https://doi.org/10.1016/j.nima.2010.04.001.

[22] Pogorelsky IV, Progress and prospects of a compton x-ray source driven by a high-power CO2 laser. In X-ray lasers 2014, Springer Proceedings in Physics, vol. 169, Springer International Publishing Switzerland; 2016. p. 133. doi:10.1007/978-3-319-195521-6.

[23] Chi Z, Yan L, Du Y, Zhang Z, Huang W, Chen H, Tang C. Recent progress of phase-contrast imaging at Tsinghua Thomson-scattering X-ray source. Nucl Instrum Methods Phys Res Sect B 2017;402:364–9. https://doi.org/10.1016/j.nimb.2017.02.062.

[24] Chi Z, Du Y, Yan L, Wang D, Zhang H, Huang W, Tang C. Experimental feasibility of dual-energy computed tomography based on the Thomson scattering X-ray source. J Synch Radiat 2018;25(6):1797–802. https://doi.org/10.1107/S1600577518012663.

[25] Luiten O. KNAW-Agenda Grootschalige Onderzoeksfaciliteiten: Smart*Light: a Dutch table-top synchrotron light source, Koninklijke Nederlandse Akademie van Wetenschappen (KNAW) (2016) 1–25. https://pure.tue.nl/ws/files/41980945/Eervol_KNAW_Agenda_SmartLight.pdf.

[26] Graves WS, Chen JPJ, Fromme P, Holl MR, Kirian R, Malin LE, et al. Asu Compact XFEL, 38th International free electron laser conference TUB03 (2017). doi:10.18429/JACoW-FEL2017-TUB03.

[27] Graves WS, Brown W, Kaertner FX, Moncton DE. MIT inverse Compton source concept. Nucl Instrum Methods Phys Res Sec A 2009;608:S103–105. https://doi.org/10.1016/j.nima.2009.05.042.

[28] Drebot I, Bacci A, Bosotti A, Broggi F, Canella F, Cardarelli P, Cialdi S, Faillace L, Galzerano G, Gambaccini M, Giannotti D, Giove D, Mettivier G, Michelato P, Monaco L, Paparella R, Paternó G, Petrillo V, Prelz F, Rossetti Conti M, Rossi AR, Russo P, Sarno A, Suerra E, Taibi A, Serafini L. BriXs ultra high flux inverse Compton source based on modified push-pull energy recovery linacs. Instruments 2019;3:49. https://doi.org/10.3390/instruments3030049.

[29] Androsov A, Drebot I, Gordienko A, Grevtsev V, Gvozd A, Ivashchenko V, et al. Status of NESTOR facility. In IPAC 2010-1st international particle accelerator conference, Kyoto, Japan, vol. WEPEA063; 2010. p. 2630–2. https://accelconf.web.cern.ch/IPAC10/papers/wepea063.pdf.

[30] Shcherbakov AA, Androsov VP, Aizatsky N, Boriskin VN, Bulyak EV, Dovbnya AN, et al. The Kharkov X-ray generator facility NESTOR. In IPAC 13-4th international particle accelerator conference, May 2013, Shanghai, China, vol. in2p3-0082; 2013. p. 2253–5. http://hal.in2p3.fr/in2p3-00823292.

[31] Schleede S. X-ray phase-contrast imaging at a compact laser-driven synchrotron source, Ph.D. thesis, Technical University of Munich (2013). URL http://mediatum.ub.tum.de/?id=1173926.

[32] Deitrick KE, Krafft GA, Terzić B, Delayen JR. High-brilliance, high-flux compact inverse Compton light source. Phys Rev Accel Beams 2018;21. https://doi.org/10.1103/PhysRevAccelBeams.21.080703. 080703.

[33] Jacobson B. Dichromatic Absorption Radiography. Dichromography. Acta Radiologica 1953;39(6):437–52. https://doi.org/10.3109/00016925309136730.

[34] Rubenstein E, Hughes EB, Campbell LE, Hofstadter R, Kirk RL, Krolicki TJ, et al. Synchrotron radiation and its application to digital subtraction angiography, in: WRBMD (Ed.), Digital radiography, vol. 0314, International society for optics and photonics, SPIE; 1981. p. 42–9. doi:10.1117/12.933021.

[35] Rubenstein E, Brown GS, Harrison DC, Kernoff RS, Otis JN, Thompson AC, Zeman HD. Synchrotron radiation for transvenous coronary angiography. Trans Am Clin Climatol Assoc 1986;97:27–31.

[36] Hughes E, Rubensteinh E, Zeman H, Brown GS, Buchbinder M, Harrison DC, Hofstadter R, Kernoff RS, Otis J, Sommer HA, Thompson AC, Walton JT. Prospects for non-invasive angiography with tunable X-rays. Nucl Instrum Methods Phys Res Sect B 1985;10–11(1):323–8. https://doi.org/10.1016/0168-583X(85)90261-7.

[37] Pelz DM, Fox AJ, Vinuela F. Digital subtraction angiography: current clinical applications. Stroke 1985;16(3):528–36. https://doi.org/10.1161/01.str.16.3.528.

[38] Thompson A, Rubenstein E, Zeman HD, Hofstadter R, Otis J, Giacomini JC, Gordon H, Brown GS, Thomlinson W, Kernoff RS. Coronary angiography using synchrotron radiation (invited). Rev Sci Instrum 1989;60(7):1674–9. https://doi.org/10.1063/1.1141056.

[39] Dix W-R. Intravenous coronary angiography with synchrotron radiation. Prog Biophys Mol Biol 1995;63:159–91. https://doi.org/10.1088/0143-0807/19/6/004.

[40] Elleaume H, Fiedler S, Estève F, Bertrand B, Charvet aM, Berkvens P, et al. First human transvenous coronary angiography at the european synchrotron radiation facility. Phys Med Biol 45 (9) (2000) L39–L43. doi:10.1088/0031-9155/45/9/102.

[41] Dix WR, Kupper W, Dill T, Hamm CW, Job H, Lohmann M, Reime B, Ventura R. Comparison of intravenous coronary angiography using synchrotron radiation with selective coronary angiography. J Synch Radiat 2003;10(3):219–27. https://doi.org/10.1107/S0909049503001973.

[42] Bertrand B, Estève F, Elleaume H, Nemoz C, Fiedler S, Bravin A, Berruyer G, Brochard T, Renier M, Machecourt J, Thomlinson W, Le Bas JF. Comparison of synchrotron radiation angiography with conventional angiography for the diagnosis of in-stent restenosis after percutaneous transluminal coronary angioplasty. Eur Heart J 2005;26(13):1284–91. https://doi.org/10.1093/eurheartj/ehi165.

[43] Schültke E, Fiedler S, Kelly M, Griebel R, Juurlink B, LeDuc G, Estève F, Le Bas JF, Renier M, Nemoz C, Meguro K. The potential for neurovascular intravenous angiography using K-edge digital subtraction angiography. Nucl Instrum Meth Phys Res A 2005;548:84–7. https://doi.org/10.1016/j.nima.2005.03.071.

[44] Thompson A, Llacer J, Campbell Finman L, Hughes E, Otis J, Wilson S, et al. Computed tomography using synchrotron radiation. Nucl Instrum Meth Phys Res 222 (1984) 319–323. doi:10.1016/0167-5087(84)90550-7.

[45] Dilmanian FA, Garrett RF, Thomlinson WC, Berman L, Chapman LD, Hastings JB, Luke PN, Oversluizen T, Siddons DP, Slatkin DN, Stojanoff V, Thompson AC, Volkow ND, Zeman HD. Computed tomography with monochromatic X-rays from the national synchrotron light source. Nucl Instrum Meth Phys Res B 1991;56: 1208–13. https://doi.org/10.1016/0168-583X(91)95133-X.

[46] Giacomini JC, Gordon H, O'Neil R, Van Kessel A, Cason B, Chapman D, Lavendar W, Gmur N, Menk R, Thomlinson W, Zhong Z, Rubenstein E. Bronchial imaging in humans using xenon K-edge dichromography. Nucl Instrum Meth Phys Res Sec A 1998;406:473–8. https://doi.org/10.1016/S0168-9002(98)00195-8.

[47] Bayat S, Le Duc G, Porra L, Berruyer G, Nemoz C, Monfraix S, Fiedler S, Thomlinson W, Suortti P, Standertskjöld-Nordenstam CG, Sovijärvi AR. Quantitative functional lung imaging with synchroton radiation using inhaled xenon as contrast agent. Phys Med Biol 2001;46:3287–99. https://doi.org/10.1088/0031-9155/46/12/315.

[48] Panahifar A, Samadi N, Swanston TM, Chapman LD, Cooper DM. Spectral K-edge subtraction imaging of experimental non-radioactive barium uptake in bone. Physica Med 2016;32:1765–70. https://doi.org/10.1016/j.ejmp.2016.07.619.

[49] Cooper DM, Carter Y, Wu Y, Panahifar A, Britz HM, Bewer B, Zhouping W, Duke MJ, Doschak M. Three dimensional mapping of strontium in bone by dual energy K-edge subtraction imaging. Phys Med Biol 2012;57:5777–86. https://doi.org/10.1088/0031-9155/57/18/5777.

[50] Kulpe S, Dierolf M, Braig E, Günther B, Achterhold K, Gleich B, Herzen J, Rummeny E, Pfeiffer F, Pfeiffer D. K-edge subtraction imaging for coronary angiography with a compact synchrotron X-ray source. PLoS ONE 2018;13(12). https://doi.org/10.1371/journal.pone.0208446. e0208446.

[51] Sarnelli A, Nemoz C, Elleaume H, Estève F, Bertrand B, Bravin A. Quantitative analysis of synchrotron radiation intravenous angiographic images. Phys Med Biol 2005;50(4):725–40. https://doi.org/10.1088/0031-9155/50/4/011.

[52] Lehmann LA, Alvarez RE, Macovski A, Brody WR, Pelc NJ, Riederer SJ, Hall AL. Generalized image combinations in dual KVP digital radiography. Med Phys 1981; 8(5):659–67. https://doi.org/10.1118/1.595025.

[53] Sarnelli A, Taibi A, Baldelli P, Gambaccini M, Bravin A. Quantitative analysis of the effect of energy separation in k-edge digital subtraction imaging. Phys Med Biol 2007;52:3015–26. https://doi.org/10.1088/0031-9155/52/11/006.

[54] Williams O, Andonian G, Babzien M, Hemsing E, Kusche K, Park J, Pogorelsky I, Priebe G, Rosenzweig J, Yakimenko V. Characterization results of the BNL ATF Compton X-ray source using K-edge absorbing foils. Nucl Instrum Meth Phys Res Sec A 2009;608(1 SUPPL.):2462–4. https://doi.org/10.1016/j.nima.2009.05.166.

[55] Golosio B, Endrizzi M, Oliva P, Delogu P, Carpinelli M, Pogorelsky I, et al. Measurement of an inverse Compton scattering source local spectrum using k-edge filters. Appl Phys Lett 100 (16) (2012). doi:10.1063/1.4703932.

[56] Carroll FE, Mendenhall MH, Traeger RH, Brau C, Waters JW. Pulsed tunable monochromatic x-ray beams from a compact source: new opportunities. Am J Roentgenol 2003;181(5):1197–202. https://doi.org/10.2214/ajr.181.5.1811197.

[57] Yamada K, Kuroda R, Toyakawa H, Ikeura-Sekiguchi H, Yasumoto M, Koike M, Sakai F, Mori K, Mori H, Fukuyama N, Sato E. A trial for fine and low-dose imaging of biological specimens using quasi-monochromatic laser-Compton X-rays. Nucl Instrum Meth Phys Res Sect A 2009;608(1):S7–10. https://doi.org/10.1016/j.nima.2009.05.157.

[58] Eggl E, Mechlem K, Braig E, Kulpe S, Dierolf M, Günther B, Achterhold K, Herzen J, Gleich B, Rummeny E, Noel PB, Pfeiffer F, Muenzel D. Mono-energy coronary angiography with a compact synchrotron source. Sci Rep 2017;7:42211. https://doi.org/10.1038/srep42211.

[59] Carroll F. Tunable, monochromatic x-rays: An enabling technology for molecular/cellular imaging and therapy. J Cell Biochem 2003;90(3):502–8. https://doi.org/10.1002/jcb.10632.

[60] Kuroda R, Taira Y, Yasumoto M, Toyokawa H, Yamada K. K-edge imaging with quasi-monochromatic LCS X-ray source on the basis of S-band compact electron linac. Nucl Instrum Meth Phys Res Sect B 2014;331:257–60. https://doi.org/10.1016/j.nimb.2014.01.034.

[61] Chi Z, Du Y, Huang W, Tang C, et al. Energy-angle correlation correction algorithm for monochromatic computed tomography based on Thomson scattering X-ray source. J Appl Phys 122 (23) (2017). doi:10.1063/1.4996324.

[62] Chi Z, Du Y, Yan L, Zhou Z, Zhang Z, Wang D, et al. Thomson scattering x-ray source: a novel tool for monochromatic computed tomography. In Proceedings volume 10391, developments in x-ray tomography XI; 2017. p. 103910Z. doi: 10.1117/12.2273136.

[63] Carroll FE. Tunable monochromatic X rays: A new paradigm in medicine. Am J Roentgenol 2002;179(3):583–90. https://doi.org/10.2214/ajr.179.3.1790583.

[64] Kulpe S, Dierolf M, Braig E-M, Günther B, Achterhold K, Gleich B, Herzen J, Rummeny E, Pfeiffer F, Pfeiffer D. K-edge subtraction imaging for iodine and calcium separation at a compact synchrotron X-ray source. J Med Imag 2020;7(2). https://doi.org/10.1117/1.JMI.7.2.023504. 023504.

[65] Kulpe S, Dierolf M, Günther B, Busse M, Achterhold K, Gleich B, Herzen J, Rummeny E, Pfeiffer F, Pfeiffer D. K-edge subtraction computed tomography with a compact synchrotron X-ray source. Sci Rep 2019;9:13332. https://doi.org/10.1038/s41598-019-49899-z.

[66] Kulpe S, Dierolf M, Benedikt G, Brantl J, Busse M, Achterhold K, Pfeiffer F, Pfeiffer D. Dynamic K-edge subtraction fluoroscopy at a compact inverse-Compton synchrotron X-ray source. Sci Rep 2020;10:9612. https://doi.org/10.1038/s41598-020-66414-x.

[67] Paternò G, Cardarelli P, Gambaccini M, Serafini L, Petrillo V, Drebot I, Taibi A. Inverse Compton radiation: a novel x-ray source for K-edge subtraction angiography? Phys Med Biol 2019;64(18). https://doi.org/10.1088/1361-6560/ab325c. 185002.

[68] Variola A, Haissinski J, Loulergue A, Zomer F. ThomX technical design report, Tech. rep., ThomX (2014). URL http://hal.in2p3.fr/in2p3-00971281.

[69] Cardarelli P, Bacci A, Calandrino R, Canella F, Castriconi R, Cialdi S, Del Vecchio A, di Franco F, Drebot I, Gambaccini M, Giannotti D, Loria A, Mettivier G, Paternò G, Petrillo V, Rossetti Conti M, Russo P, Sarno A, Suerra E, Taibi A, Serafini L. BriXS, a new X-ray inverse Compton source for medical applications. Physica Med 2020;77: 127–37. https://doi.org/10.1016/j.ejmp.2020.08.013.

[70] Thomas JV, Bolus DN, Jackson BE, Berland LL, Yester M, Morgan DE. Gadoxetate disodium enhanced spectral dual-energy CT for evaluation of cholangiocarcinoma: Preliminary data. Ann Med Surg 2016;6:17–22. https://doi.org/10.1016/j.amsu.2016.01.001.

[71] van Hamersvelt RW, Willemink MJ, de Jong PA, Milles J, Vlassenbroek A, Schilham AM, Leiner T. Feasibility and accuracy of dual-layer spectral detector computed tomography for quantification of gadolinium: a phantom study. Eur Radiol 2017;27(9):3677–86. https://doi.org/10.1007/s00330-017-4737-8.

[72] Sam AD, Morasch MD, Collins J, Song G, Chen R, Pereles FS. Safety of gadolinium contrast angiography in patients with chronic renal insufficiency. J Vasc Surg 2003;38(2):313–8. https://doi.org/10.1016/S0741-5214(03)00315-X.

[73] Sayin T, Turhan S, Akyürek O, Kilickap M. Gadolinium:nonionic contrast media (1: 1) coronary angiography in patients with impaired renal function. Angiology 2007; 58(5):561–4. https://doi.org/10.1177/0003319707303640.

[74] Patel M, Atyani A, Salameh J-P, McInnes M, Chakraborty S. Safety of Intrathecal Administration of Gadolinium-based contrast agents: a systematic review and meta-analysis title. Radiology 297 (1) (2020). doi:10.1148/radiol.2020191373.

[75] Achterhold K, Bech M, Schleede S, Potdevin G, Ruth R, Loewen R, et al. Monochromatic computed tomography with a compact laser-driven X-ray source. Sci Rep 2013;3:1313. https://doi.org/10.1038/srep01313.